

## Modal analysis of eccentric shells with fluid-filled annulus

Myung Jo Jhung<sup>†</sup>

*Korea Institute of Nuclear Safety, 19 Kusong-dong, Yusong-gu, Daejeon 305-338, Korea*

Kyeong Hoon Jeong<sup>†</sup>

*Korea Atomic Energy Research Institute, 150 Dukjin-dong, Yusong-gu, Daejeon 305-353, Korea*

Won Gul Hwang<sup>‡</sup>

*Chonnam National University, 300 Yongbong-dong, Puk-gu, Kwangju 500-757, Korea*

*(Received May 8, 2000, Accepted May 3, 2002)*

**Abstract.** Investigated in this study are the modal characteristics of the eccentric cylindrical shells with fluid-filled annulus. Theoretical method is developed to find the natural frequencies of the shell using the finite Fourier expansion, and their results are compared with those of finite element method to verify the validation of the method developed. The effect of eccentricity on the modal characteristics of the shells is investigated using a finite element modeling.

**Key words:** cylindrical shell; modal characteristic; fluid-filled annulus; finite element method; eccentricity.

---

### 1. Introduction

A fluid-surrounded cylindrical shells subjected to various loads have been widely used as structural components in the engineering design. One example is reactor internals such as core barrel and upper structure barrel coupled with each other by fluid-filled annulus (Song and Jhung 1999). To assure the reliability of those components and to verify structural integrity during normal operations of a nuclear power plant (Jhung 1996), it is necessary to investigate extensively flow-induced vibration, necessitating the investigation of the modal characteristics. Several monitoring systems such as internal vibration monitoring system using neutron noise analysis are employed to find in advance the defect which may cause severe damage on the reactor internals and steam generator and to take actions to prevent such damage in time. One of major causes for accidents is the eccentricity of inner shell when it is submerged in a fluid which came from the failure of connections to other major components.

---

<sup>†</sup> Principal Researcher

<sup>‡</sup> Professor

Several previous investigations have been performed to analyze the free vibration of fluid-filled, coaxial cylindrical shells (Chen and Rosenberg 1975, Yoshikawa *et al.* 1994), which were limited to the approximated methods and could provide only the in-phase and out-of-phase modes of coaxial shells with small annular fluid gap compared to the shell diameters. Therefore, an advanced general theory was developed to calculate the natural frequencies for all vibrational modes of two coaxial circular cylindrical shells coupled with fluid (Jhung 2000). Even though coaxial shells are extensively studied very few studies of eccentric shells are found. Danila *et al.* (1995) suggested a calculating method of the scattered field due to a plane wave incident on one or several cylindrical fluid-fluid interfaces using the generalized Debye series expansion. The theoretical method is applied to a concentric and a non-concentric fluid shell and then extended to the multi-layered cylindrical structure. However, few theoretical studies on the free vibration of a circular cylindrical shell submerged in a compressible fluid-filled cylindrical container were taken into consideration.

This study develops an advanced general theory to calculate the natural frequencies for all vibrational modes of two eccentric circular cylindrical shells with fluid-filled annulus. To support the validity of the proposed theory, finite element analyses are carried out for various eccentricities. The effect of eccentricity on the natural frequencies of the shells is investigated by comparing frequencies according to the eccentricity.

## 2. Theory

### 2.1 Equation of motion

Consider a circular cylindrical shell with a clamped boundary condition at both ends, as illustrated in Fig. 1. The shell can be concentrically or eccentrically submerged in a fluid-filled container. The cylindrical shell has mean radius  $R$ , height  $L$ , and wall thickness  $h$ . The Sanders' shell equations (Jeong and Lee 1996, Jeong 1998) as the governing equations for the shell where the hydrodynamic effects are considered, can be written as :

$$R^2 u_{,xx} + \frac{(1-\mu)}{2} \left(1 + \frac{k}{4}\right) u_{,\theta\theta} + R \left( \frac{(1-\mu)}{2} - \frac{3(1-\mu)}{8} k \right) v_{,x\theta} + \mu R w_{,x} + \frac{(1-\mu)}{2} R k w_{,x\theta\theta} = \gamma^2 u_{,tt} \quad (1a)$$

$$R \left( \frac{(1-\mu)}{2} - \frac{3(1-\mu)}{8} k \right) u_{,x\theta} + (1+k) v_{,\theta\theta} + \frac{(1-\mu)}{2} R^2 \left(1 + \frac{9k}{4}\right) v_{,xx} - \frac{(3-\mu)}{2} R^2 k w_{,xx\theta} + w_{,\theta} - k w_{,\theta\theta\theta} = \gamma^2 v_{,tt} \quad (1b)$$

$$\frac{(1-\mu)}{2} R k u_{,x\theta\theta} + \mu R u_{,x} - \frac{(3-k)}{2} R^2 k v_{,xx\theta} + v_{,\theta} + w + k(R^4 w_{,xxxx} + 2R^2 w_{,xx\theta\theta} + w_{,\theta\theta\theta\theta} - v_{,\theta\theta\theta}) = -\gamma^2 u_{,tt} + \frac{R^2 p}{D} \quad (1c)$$

where  $D = Eh/(1-\mu^2)$ ,  $k = h^2/12R^2$ ,  $\gamma^2 = \rho R^2(1-\mu^2)/E$ ,  $\mu$  Poisson's ratio,  $p$  dynamic liquid



where  $M_x$  and  $N_x$  denote the bending moment and the membrane tensile force, respectively. All geometric boundary conditions applicable to the clamped-clamped shell can be reduced to the following equations for the ends of the shell (Jeong and Kim 1998):

$$v(0) = w(0) = v(L) = w(L) = 0. \quad (3)$$

The relationships between the boundary forces and displacements are

$$N_x = D \left[ u_{,x} + \frac{\mu}{R} v_{,\theta} + \frac{\mu}{R} w \right] \quad (4a)$$

$$N_{x\theta} = \frac{D(1-\mu)}{2} \left[ \frac{1}{R} \left( 1 - \frac{3}{4}k \right) u_{,\theta} + \left( 1 + \frac{9}{4}k \right) v_{,x} - 3k w_{,x\theta} \right] \quad (4b)$$

$$Q_x = K \left[ -\frac{(1-\mu)}{2R^3} u_{,\theta\theta} + \frac{(3-\mu)}{2R^2} v_{,x\theta} - \frac{(2-\mu)}{R^2} w_{,x\theta\theta} - w_{,xxx} \right] \quad (4c)$$

$$M_x = K \left[ \frac{\mu}{R^2} (v_{,\theta} - w_{,\theta\theta}) - w_{,xx} \right] \quad (4d)$$

where  $K = Eh^3/12(1-\mu^2)$ .  $N_{x\theta}$  and  $Q_x$  denote the membrane shear force and transverse shear force per unit length, respectively.

## 2.2 Modal functions

A general relation for the dynamic displacements in any vibration mode of the shell can be written in the following form for the cylindrical coordinate  $r, \theta$ .

$$u(x, \theta, t) = u(x, \theta) \exp(i\omega t) \quad (5a)$$

$$v(x, \theta, t) = v(x, \theta) \exp(i\omega t) \quad (5b)$$

$$w(x, \theta, t) = w(x, \theta) \exp(i\omega t) \quad (5c)$$

where  $u(x, \theta)$ ,  $v(x, \theta)$ , and  $w(x, \theta)$  are modal functions corresponding to the axial, tangential, and radial displacements for the shell, respectively. These modal functions along the axial direction can be described by a sum of linear combinations of the Fourier series that are orthogonal.

$$u(x, \theta) = \sum_{n=1}^{\infty} \sum_{s=1}^{\infty} A_{sn} \sin\left(\frac{s\pi x}{L}\right) \cos n\theta \quad (6a)$$

$$v(x, \theta) = \sum_{n=1}^{\infty} \left[ B_{on} + \sum_{s=1}^{\infty} B_{sn} \cos\left(\frac{s\pi x}{L}\right) \right] \sin n\theta \quad (6b)$$

$$w(x, \theta) = \sum_{n=1}^{\infty} \left[ C_{on} + \sum_{s=1}^{\infty} C_{sn} \cos\left(\frac{s\pi x}{L}\right) \right] \cos n\theta \quad (6c)$$

The derivatives of the above modal functions for the shell can be obtained using the finite Fourier transformation (Jeong and Kim 1998, Sneddon 1951). The modal functions and their derivatives of

the cylindrical shell were described in Jeong and Kim (1998).

### 2.3 Equation of fluid motion

The inviscid, irrotational and compressible fluid movement due to shell vibration is described by the Helmholtz equation :

$$\Phi_{,rr} + \frac{1}{r}\Phi_{,r} + \frac{1}{r^2}\Phi_{,\theta\theta} + \Phi_{,xx} = \frac{1}{c^2}\Phi_{,tt} \quad (7)$$

where  $c$  is the speed of sound in the fluid medium equal to  $\sqrt{B/\rho_0}$ ,  $B$  is the bulk modulus of elasticity of fluid and  $\rho_0$  stands for the fluid density. It is possible to separate the function  $\Phi$  with respect to  $x$  by observing that, in the axial direction, the rigid surfaces support the edges of the shell; thus

$$\Phi(x, r, \theta, t) = i\omega\phi(r, \theta, x)\exp(i\omega t) = i\omega\eta(r, \theta)f(x)\exp(i\omega t) \quad (8)$$

where  $\omega$  is the fluid-coupled frequency of the shell. Substitution of Eq. (8) into the partial differential Eq. (7) gives

$$\frac{\eta(r, \theta)_{,rr} + \frac{1}{r}\eta(r, \theta)_{,r} + \frac{1}{r^2}\eta(r, \theta)_{,\theta\theta} + \left(\frac{\omega}{c}\right)^2\eta(r, \theta)}{\eta(r, \theta)} = \frac{f(x)_{,xx}}{f(x)} = \left(\frac{s\pi}{L}\right)^2 \quad (9)$$

It is possible to solve the partial differential Eq. (9) by the separation of the variables. The solution can be obtained with respect to the original cylindrical coordinates,  $r$ ,  $\theta$  and  $x$ ;

for  $\frac{s\pi}{L} \geq \frac{\omega}{c}$ ,

$$\phi(r, \theta, x) = \sum_{n=1}^{\infty} \left[ D_{on}J_n\left(\frac{\omega r}{c}\right) + F_{on}Y_n\left(\frac{\omega r}{c}\right) + \sum_{s=1}^{\infty} \{D_{sn}I_n(\alpha_{sn}r) + F_{sn}K_n(\alpha_{sn}r)\} \cos\left(\frac{s\pi x}{L}\right) \right] \sin n\theta \quad (10a)$$

and for  $\frac{s\pi}{L} < \frac{\omega}{c}$

$$\phi(r, \theta, x) = \sum_{n=1}^{\infty} \left[ D_{on}J_n\left(\frac{\omega r}{c}\right) + F_{on}Y_n\left(\frac{\omega r}{c}\right) + \sum_{s=1}^{\infty} \{D_{sn}J_n(\alpha_{sn}r) + F_{sn}Y_n(\alpha_{sn}r)\} \cos\left(\frac{s\pi x}{L}\right) \right] \sin n\theta \quad (10b)$$

where  $J_n$  and  $Y_n$  are Bessel functions of the first and second kinds of order  $n$ , whereas  $I_n$  and  $K_n$  are modified Bessel functions of the first and second kinds of order  $n$ .  $\phi$  means the spatial velocity potential of the contained compressible fluid.  $\alpha_{sn}$  is related to the speed of sound in the fluid medium as follows;

$$\alpha_{sn} = \sqrt{\left(\frac{s\pi}{L}\right)^2 - \left(\frac{\omega}{c}\right)^2} \quad \text{for } s = 1, 2, 3, \dots \quad (11)$$

The Eqs. (10a) and (10b) automatically satisfy the boundary conditions that appear as follows:

(a) impermeable rigid surface on the bottom is

$$\frac{\partial \phi(r, \theta, x)}{\partial x} = 0 \quad \text{at } x=0 \quad (12)$$

(b) as there exists no free surface, the axial fluid velocity at the rigid top is also zero, so

$$\frac{\partial \phi(r, \theta, x)}{\partial x} = 0 \quad \text{at } x=L \quad (13)$$

#### 2.4 General formulation

For the eccentrically submerged shell, the velocity potential of Eqs. (10a) and (10b) can be transformed to the shifted cylindrical coordinates,  $(a, \psi, x)$  by Graf's addition theorem and Beltrami's theorem (Watson 1980);

for  $\frac{s\pi}{L} \geq \frac{\omega}{c}$ ,

$$\phi(a, \psi, x) = \sum_{n=1}^{\infty} \sum_{m=-\infty}^{\infty} \left[ \begin{aligned} & \left\{ D_{on} J_{n+m} \left( \frac{\omega a}{c} \right) + F_{on} Y_{n+m} \left( \frac{\omega a}{c} \right) \right\} J_m \left( \frac{\omega \varepsilon}{c} \right) \\ & + \sum_{s=1}^{\infty} \left\{ D_{sn} (-1)^m I_{n+m}(\alpha_{sn} a) + F_{sn} K_{n+m}(\alpha_{sn} a) \right\} \\ & \times I_m(\alpha_{sn} \varepsilon) \cos \left( \frac{s\pi x}{L} \right) \end{aligned} \right] \sin m\psi \quad (14a)$$

for  $\frac{s\pi}{L} < \frac{\omega}{c}$ ,

$$\phi(a, \psi, x) = \sum_{n=1}^{\infty} \sum_{m=-\infty}^{\infty} \left[ \begin{aligned} & \left\{ D_{on} J_{n+m} \left( \frac{\omega a}{c} \right) + F_{on} Y_{n+m} \left( \frac{\omega a}{c} \right) \right\} J_m \left( \frac{\omega \varepsilon}{c} \right) \\ & + \sum_{s=1}^{\infty} \left\{ D_{sn} J_{n+m}(\alpha_{sn} a) + F_{sn} Y_{n+m}(\alpha_{sn} a) \right\} \\ & \times J_m(\alpha_{sn} \varepsilon) \cos \left( \frac{s\pi x}{L} \right) \end{aligned} \right] \sin m\psi \quad (14b)$$

It is convenient to handle the boundary condition along the surface of the rigid container when the velocity potential is transformed from the origin "O" to the shifted origin "O'". The radial fluid velocity along the outer wetted surface of the shell must be identical to that of the flexible shell, so

$$\frac{\partial \phi(r, \theta, x)}{\partial r} = -w(x, \theta) \quad \text{at } r=R \quad (15)$$

Additionally, the radial fluid velocity along the wetted surface of the outer rigid container that maintains eccentricity to the shell must be zero, so

$$\frac{\partial \phi(x, \psi, a)}{\partial a} = 0 \quad \text{at } a=R_0 \quad (16)$$

Substitution of Eqs. (6c), (14a) and (14b) into Eqs. (15) and (16) gives the relationships:

for  $\frac{s\pi}{L} \geq \frac{\omega}{c}$ ,

$$\begin{aligned} & \sum_{n=1}^{\infty} \left[ \begin{aligned} & \left( \frac{\omega}{c} \right) \left\{ D_{on} J_n' \left( \frac{\omega R}{c} \right) + F_{on} Y_n' \left( \frac{\omega R}{c} \right) \right\} \\ & + \sum_{s=1}^{\infty} \alpha_{sn} \{ D_{sn} I_n' (\alpha_{sn} R) + F_{sn} K_n' (\alpha_{sn} R) \} \cos \left( \frac{s\pi x}{L} \right) \end{aligned} \right] \cos n\theta \\ & = - \sum_{n=1}^{\infty} \left[ C_{on} + \sum_{s=1}^{\infty} C_{sn} \cos \left( \frac{s\pi x}{L} \right) \right] \cos n\theta \end{aligned} \quad (17a)$$

for  $\frac{s\pi}{L} < \frac{\omega}{c}$ ,

$$\begin{aligned} & \sum_{n=1}^{\infty} \left[ \begin{aligned} & \left( \frac{\omega}{c} \right) \left\{ D_{on} J_n' \left( \frac{\omega R}{c} \right) + F_{on} Y_n' \left( \frac{\omega R}{c} \right) \right\} \\ & + \sum_{s=1}^{\infty} \alpha_{sn} \{ D_{sn} J_n' (\alpha_{sn} R) + F_{sn} Y_n' (\alpha_{sn} R) \} \cos \left( \frac{s\pi x}{L} \right) \end{aligned} \right] \cos n\theta \\ & = - \sum_{n=1}^{\infty} \left[ C_{on} + \sum_{s=1}^{\infty} C_{sn} \cos \left( \frac{s\pi x}{L} \right) \right] \cos n\theta \end{aligned} \quad (17b)$$

for  $\frac{s\pi}{L} \geq \frac{\omega}{c}$ ,

$$\begin{aligned} & \sum_{m=-\infty}^{\infty} \left[ \begin{aligned} & \left( \frac{\omega}{c} \right) J_m \left( \frac{\omega \varepsilon}{c} \right) \left\{ D_{on} J_{n+m}' \left( \frac{\omega R_0}{c} \right) + F_{on} Y_{n+m}' \left( \frac{\omega R_0}{c} \right) \right\} \\ & + \sum_{s=1}^{\infty} \alpha_{sn} I_m (\alpha_{sn} \varepsilon) \{ D_{sn} (-1)^m I_{n+m}' (\alpha_{sn} R_0) + F_{sn} K_{n+m}' (\alpha_{sn} R_0) \} \\ & \times \cos \left( \frac{s\pi x}{L} \right) \end{aligned} \right] = 0 \end{aligned} \quad (18a)$$

for  $\frac{s\pi}{L} < \frac{\omega}{c}$ ,

$$\begin{aligned} & \sum_{m=-\infty}^{\infty} \left[ \begin{aligned} & \left( \frac{\omega}{c} \right) J_m \left( \frac{\omega \varepsilon}{c} \right) \left\{ D_{on} J_{n+m}' \left( \frac{\omega R_0}{c} \right) + F_{on} Y_{n+m}' \left( \frac{\omega R_0}{c} \right) \right\} \\ & + \sum_{s=1}^{\infty} \alpha_{sn} J_m (\alpha_{sn} \varepsilon) \{ D_{sn} J_{n+m}' (\alpha_{sn} R_0) + F_{sn} Y_{n+m}' (\alpha_{sn} R_0) \} \\ & \times \cos \left( \frac{s\pi x}{L} \right) \end{aligned} \right] = 0 \end{aligned} \quad (18b)$$

Now, all unknown coefficients  $D_{on}$ ,  $F_{on}$ ,  $D_{sn}$ , and  $F_{sn}$  related to the fluid motion will be written in terms of the coefficients  $C_{on}$  and  $C_{sn}$  related to the shell motion using Eqs. (17a), (17b), (18a), and (18b).

$$F_{on} = W_{n1}D_{on} \quad (19a)$$

$$D_{on} = \Gamma_{n1}C_{on} \quad (19b)$$

$$F_{on} = \Gamma_{n2}C_{on} \quad (19c)$$

$$\text{For } \frac{s\pi}{L} \geq \frac{\omega}{c},$$

$$F_{sn} = W_{n2}D_{sn} \quad (19d)$$

$$D_{sn} = \Gamma_{sn3}C_{sn} \quad (19e)$$

$$F_{sn} = \Gamma_{sn5}C_{sn} \quad (19f)$$

$$\text{For } \frac{s\pi}{L} < \frac{\omega}{c}$$

$$F_{sn} = W_{n3}D_{sn} \quad (19g)$$

$$D_{sn} = \Gamma_{sn4}C_{sn} \quad (19h)$$

$$F_{sn} = \Gamma_{sn6}C_{sn} \quad (19i)$$

where

$$W_{n1} = -\frac{\sum_{m=-\infty}^{\infty} \left\{ J_m\left(\frac{\omega\varepsilon}{c}\right) J_{n+m}'\left(\frac{\omega R_0}{c}\right) \right\}}{\sum_{m=-\infty}^{\infty} \left\{ J_m\left(\frac{\omega\varepsilon}{c}\right) Y_{n+m}'\left(\frac{\omega R_0}{c}\right) \right\}} \quad (20a)$$

$$W_{n2} = -\frac{\sum_{m=-\infty}^{\infty} \{ I_m(\alpha_{sn}\varepsilon)(-1)^m I_{n+m}'(\alpha_{sn}R_0) \}}{\sum_{m=-\infty}^{\infty} \{ I_m(\alpha_{sn}\varepsilon) K_{n+m}'(\alpha_{sn}R_0) \}} \quad (20b)$$

$$W_{n3} = -\frac{\sum_{m=-\infty}^{\infty} \{ J_m(\alpha_{sn}\varepsilon) J_{n+m}'(\alpha_{sn}R_0) \}}{\sum_{m=-\infty}^{\infty} \{ J_m'(\alpha_{sn}\varepsilon) Y_{n+m}'(\alpha_{sn}R_0) \}} \quad (20c)$$

$$\Gamma_{n1} = -\left(\frac{c}{\omega}\right) \left[ J_n'\left(\frac{\omega R}{c}\right) + W_{n1} Y_n'\left(\frac{\omega R}{c}\right) \right]^{-1} \quad (20d)$$

$$\Gamma_{n2} = W_{n1} \Gamma_{n1} \quad (20e)$$

$$\Gamma_{sn3} = \frac{-1}{\alpha_{sn} [I_n'(\alpha_{sn}R) + W_{n2} K_n'(\alpha_{sn}R)]} \quad (20f)$$

$$\Gamma_{sn4} = \frac{-1}{\alpha_{sn}[J'_n(\alpha_{sn}R) + W_{n3}Y'_n(\alpha_{sn}R)]} \quad (20g)$$

$$\Gamma_{sn5} = W_{n2}\Gamma_{sn3} \quad (20h)$$

$$\Gamma_{sn6} = W_{n3}\Gamma_{sn4} \quad (20i)$$

As the eccentric distance  $\varepsilon$  approaches zero,  $J_m(\alpha_{sn}\varepsilon)$  and  $I_m(\alpha_{sn}\varepsilon)$  of Eqs. (20a)-(20c) will be zero for  $m \neq 0$  and  $J_m(\alpha_{sn}\varepsilon) = I_m(\alpha_{sn}\varepsilon) = 1$  for  $m = 0$ . Therefore, when  $\varepsilon = 0$ , Eq. (20) for the eccentric arrangement of the shell obviously reduces to the equation of the concentric case. The concentrically submerged shell will be a special case of the shell submerged eccentrically in a fluid-filled container.

When the hydrostatic pressure on the shell are neglected for simple formulation, the hydrodynamic pressure along the outer wetted shell surface can be given by

$$p(x, \theta, t) = \rho_0 \omega^2 \phi(R, \theta, x) \exp(i\omega t) \quad (21)$$

Finally, the hydrodynamic force on the shell can be written as

for  $\frac{s\pi}{L} \geq \frac{\omega}{c}$ ,

$$\frac{R^2 p(x, \theta, t)}{D} = \frac{\rho_0 \omega^2 R^2}{D} \sum_{n=1}^{\infty} \left[ \begin{array}{l} C_{on} \left\{ \Gamma_{n1} J_n\left(\frac{\omega R}{c}\right) + \Gamma_{n2} Y_n\left(\frac{\omega R}{c}\right) \right\} \\ + \sum_{s=1}^{\infty} C_{sn} \{ \Gamma_{sn3} J_n(\alpha_{sn}R) + \Gamma_{sn5} K_n(\alpha_{sn}R) \} \end{array} \right] \exp(i\omega t) \quad (22a)$$

for  $\frac{s\pi}{L} < \frac{\omega}{c}$ ,

$$\frac{R^2 p(x, \theta, t)}{D} = \frac{\rho_0 \omega^2 R^2}{D} \sum_{n=1}^{\infty} \left[ \begin{array}{l} C_{on} \left\{ \Gamma_{n1} J_n\left(\frac{\omega R}{c}\right) + \Gamma_{n2} Y_n\left(\frac{\omega R}{c}\right) \right\} \\ + \sum_{s=1}^{\infty} C_{sn} \{ \Gamma_{sn4} J_n(\alpha_{sn}R) + \Gamma_{sn6} Y_n(\alpha_{sn}R) \} \end{array} \right] \exp(i\omega t) \quad (22b)$$

The dynamic displacements and their derivatives can be represented by a Fourier sine and cosine series in an open range of  $0 < x < L$  and with the end values using the finite Fourier transformation (Sneddon 1951). Substitution of the displacements and their derivatives into the governing Sanders' shell Eqs. (1a), (1b), and (1c), leads to an explicit relation for  $C_{on}$  and a set of equations for  $A_{sn}$ ,  $B_{sn}$ , and  $C_{sn}$  as follows :

$$\begin{bmatrix} B_{on} \\ C_{on} \end{bmatrix} = \mathbf{y}_1[u_0 + u_l] + \mathbf{y}_2[v_0 + v_l] + \mathbf{y}_3[\tilde{w}_0 + \tilde{w}_l] + \mathbf{y}_4[\tilde{\tilde{w}}_0 + \tilde{\tilde{w}}_l] \quad (23)$$

$$\begin{bmatrix} A_{sn} \\ B_{sn} \\ C_{sn} \end{bmatrix} = \mathbf{y}_5[u_0 + (-1)^m u_l] + \mathbf{y}_6[v_0 + (-1)^m v_l] + \mathbf{y}_7[\tilde{w}_0 + (-1)^m \tilde{w}_l] + \mathbf{y}_8[\tilde{\tilde{w}}_0 + (-1)^m \tilde{\tilde{w}}_l] \quad (24)$$

where the end values  $u_0, u_l, v_0, v_l, \tilde{w}_0, \tilde{w}_l, \tilde{\tilde{w}}_0$  and  $\tilde{\tilde{w}}_l$  in Eqs. (23) and (24) are defined in Jeong and Kim (1998). The matrix  $y_1, y_2, \dots, y_8$  are the derived column matrices. The equivalent hydrodynamic mass effect on the shell is included in the coefficient. The forces  $N_{x\theta}$  and  $Q_x$  at the ends of the shells can be written as a combination of some boundary values of displacement and their derivatives using Eq. (4). The boundary values of displacement and their derivatives,  $v_0, v_l, \tilde{\tilde{w}}_0$ , and  $\tilde{\tilde{w}}_l$  can be transformed in a combination of the boundary values of  $u, \tilde{w}, N_{x\theta}$ , and  $Q_x$  by Eq. (4), as written in the form

$$v_0 = g_1 u_0 + g_2 \tilde{w}_0 + g_3 N_{x\theta}^0 \quad (25a)$$

$$v_l = g_1 u_l + g_2 \tilde{w}_l + g_3 N_{x\theta}^l \quad (25b)$$

$$\tilde{\tilde{w}}_0 = g_4 u_0 + g_5 \tilde{w}_0 + g_6 N_{x\theta}^0 + g_7 Q_x^0 \quad (25c)$$

$$\tilde{\tilde{w}}_l = g_4 u_l + g_5 \tilde{w}_l + g_6 N_{x\theta}^l + g_7 Q_x^l \quad (25d)$$

where the end values of the forces are defined in reference [10] and  $g_k (k = 1, 2, \dots, 7)$  can be derived. Substitution of Eq. (25) into Eqs. (23) and (24), gives

$$\begin{bmatrix} B_{on} \\ C_{on} \end{bmatrix} = z_1 [u_0 + u_l] + z_2 [\tilde{w}_0 + \tilde{w}_l] + z_3 [N_{x\theta}^0 + N_{x\theta}^l] + z_4 [Q_x^0 + Q_x^l] \quad (26a)$$

$$\begin{bmatrix} A_{sn} \\ B_{sn} \\ C_{sn} \end{bmatrix} = [\Lambda_{ik}] \begin{bmatrix} u_0 + (-1)^m u_l \\ \tilde{w}_0 + (-1)^m \tilde{w}_l \\ N_{x\theta}^0 + (-1)^m N_{x\theta}^l \\ Q_x^0 + (-1)^m Q_x^l \end{bmatrix} \quad (26b)$$

where  $z_k (k = 1, 2, 3, 4)$  in Eq. (26a) are the derived coefficient matrices, and  $[\Lambda_{ik}]$  ( $i = 1, 2, 3$  and  $k = 1, 2, 3, 4$ ) in Eq. (26b) is the  $4 \times 3$  derived coefficients matrix. Eventually, all Fourier coefficients  $A_{sn}, B_{sn}$ , and  $C_{sn}$  are rearranged with a combination of the end point values, as shown in Eq. (26b).

The geometric boundary conditions that must be satisfied are associated with the dynamic displacement  $v$  and  $w$  as described in Eq. (3). Hence it follows that

$$v(0) = \sum_{n=1}^{\infty} \left[ B_{on} + \sum_{s=1}^{\infty} B_{sn} \right] = 0 \quad (27a)$$

$$v(L) = \sum_{n=1}^{\infty} \left[ B_{on} + \sum_{s=1}^{\infty} B_{sn} (-1)^m \right] = 0 \quad (27b)$$

$$w(0) = \sum_{n=1}^{\infty} \left[ C_{on} + \sum_{s=1}^{\infty} C_{sn} \right] = 0 \quad (27c)$$

$$w(L) = \sum_{n=1}^{\infty} \left[ C_{on} + \sum_{s=1}^{\infty} C_{sn} (-1)^m \right] = 0 \quad (27d)$$

Substitution of Eq. (26) for the coefficients  $B_{on}$ ,  $C_{on}$ ,  $A_{sn}$ ,  $B_{sn}$ , and  $C_{sn}$  into the four constraint conditions that come from the geometric boundary condition, written as Eq. (27), leads to a homogeneous matrix equation by omitting the details :

$$\begin{bmatrix} e_{11} & e_{12} & e_{13} & e_{14} & e_{15} & e_{16} & e_{17} & e_{18} \\ e_{21} & e_{22} & e_{23} & e_{24} & e_{25} & e_{26} & e_{27} & e_{28} \\ e_{31} & e_{32} & e_{33} & e_{34} & e_{35} & e_{36} & e_{37} & e_{38} \\ e_{41} & e_{42} & e_{43} & e_{44} & e_{45} & e_{46} & e_{47} & e_{48} \end{bmatrix} \begin{Bmatrix} u_0 \\ u_l \\ \tilde{w}_0 \\ \tilde{w}_l \\ N_{x\theta}^0 \\ N_{x\theta}^l \\ Q_x^0 \\ Q_x^l \end{Bmatrix} = \{0\} \quad (28)$$

The elements of the matrix,  $e_{ik}$  ( $i = 1, 2, 3, 4$  and  $k = 1, 2, \dots, 8$ ) can be obtained from Eq. (27). However, when the cylindrical shell is clamped at both support ends, the associated boundary condition is

$$u = v = w = w_{,x} = 0 \quad \text{at } x = 0 \text{ and } L \quad (29)$$

Among these boundary conditions, the two geometric boundary conditions  $u = 0$  and  $\tilde{w}_0 = 0$  at  $x = 0$  and  $x = L$  are not automatically satisfied by Eq. (6), the modal functions set. Therefore the first, second, third, and fourth rows of the matrix in Eq. (28) are enforced and the terms associated with  $u_0$ ,  $u_l$ ,  $\tilde{w}_0$ , and  $\tilde{w}_l$  are released. The  $4 \times 4$  frequency determinant is obtained from Eqs. (28) and (29) by retaining the rows and columns associated with  $N_{x\theta}^0$ ,  $N_{x\theta}^l$ ,  $Q_x^0$  and  $Q_x^l$ . For the clamped boundary condition, the coupled natural frequencies are numerically obtained from the frequency determinant:

$$\begin{vmatrix} e_{15} & e_{16} & e_{17} & e_{18} \\ e_{25} & e_{26} & e_{27} & e_{28} \\ e_{35} & e_{36} & e_{37} & e_{38} \\ e_{45} & e_{46} & e_{47} & e_{48} \end{vmatrix} = 0 \quad (30)$$

### 3. Analysis

#### 3.1 Theoretical analysis

On the basis of the preceding analysis, the frequency determinant is numerically solved for the clamped boundary condition in order to find the natural frequencies of the eccentric circular cylindrical shells with a fluid-filled annulus. The inner and outer shells are coupled with a fluid-filled annular gap. The inner cylindrical shell has a mean radius of 100 mm, a length of 300 mm,

Table 1 Dimensions and material properties

	Unit	Shell		Fluid
		Inner	Outer	
Length	m	0.300	0.300	
Mean radius	m	0.100	0.130	
Thickness	m	0.002	0.002	
Young's modulus	Pa	69E9	69E9	
Poisson's ratio		0.3	0.3	
Density	kg/m <sup>3</sup>	2700	2700	1000
Sound speed	m/sec			1483
Bulk modulus of elasticity	Pa			2.2E9

and a wall thickness of 2 mm. The outer cylindrical shell has a mean radius of 130 mm with the same length and wall thickness. The physical properties of the shell material are as follows: Young's modulus = 69.0 GPa, Poisson's ratio = 0.3, and mass density = 2700 kg/m<sup>3</sup>. Water is used as the contained fluid with a density of 1000 kg/m<sup>3</sup>. The sound speed in water, 1483 m/s, is equivalent to the bulk modulus of elasticity, 2.2 GPa. Dimensions and material properties used for the analysis are shown in Table 1.

The frequency equation derived in the preceding section involves the double infinite series of algebraic terms. Before exploring the analytical method for obtaining the natural frequencies of the fluid-coupled shells, it is necessary to conduct convergence studies and establish the number of terms required in the series expansions involved. In the numerical calculation, the Fourier expansion term  $m$  is set at 100, which gives an exact enough solution by convergence.

### 3.2 Finite element analysis

Finite element analyses using a commercial computer code ANSYS 5.5 (ANSYS 1998) are performed to verify the analytical results for the theoretical study. The finite element method results are used as the baseline data. Three-dimensional model is constructed for the finite element analysis. The fluid region is divided into a number of identical 3-dimensional contained fluid elements (FLUID80) with eight nodes having three degrees of freedom at each node. The fluid element FLUID80 is particularly well suited for calculating hydrostatic pressures and fluid/solid interactions. The circular cylindrical shell is modeled as elastic shell elements (SHELL63) with four nodes. The model has 3840 (radially  $4 \times$  axially  $20 \times$  circumferentially 48) fluid elements and 1920 shell elements as shown in Fig. 2.

The fluid boundary conditions at the top and bottom of the tank are zero displacement and rotation. The nodes connected entirely by the fluid elements are free to move arbitrarily in three-dimensional space, with the exception of those, which are restricted to motion in the bottom and top surfaces of the fluid cavity. The radial velocities of the fluid nodes along the wetted shell surfaces coincide with the corresponding velocities of the shells. Clamped-clamped boundary conditions at both ends are considered for the inner shell. The outer shell is considered to be rigid with zero displacement and rotation.

Sufficient number of master degree of freedoms is selected to calculate 200 frequencies and the

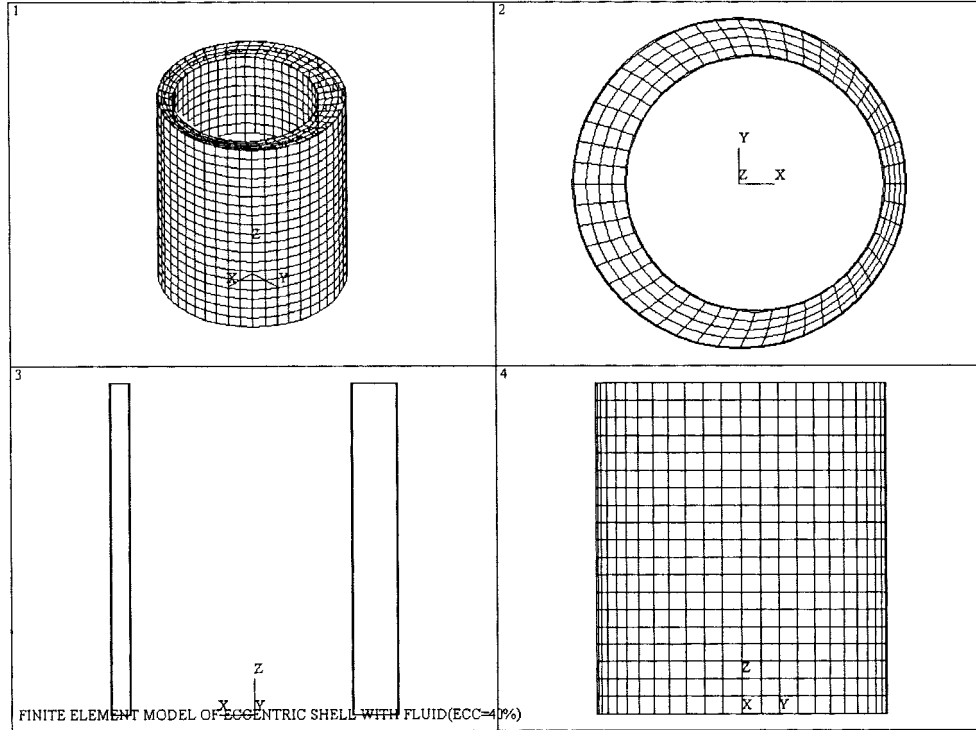


Fig. 2 Finite element model of cylindrical shells with fluid-filled annulus

reduced method is used for the eigenvalue and eigenvector extractions, which employ the Householder-Bisection-Inverse iteration extraction technique.

#### 4. Results and discussion

Mode shapes of the fluid-coupled shells are obtained by the finite element method and typical modes are plotted in Fig. 3, which shows the deformed mode shape of the fluid and shell elements for the modes of (1, 3), (2, 4), (3, 5) and (4, 5).

The frequency comparisons between analytical solution developed here and finite element method are shown in Fig. 4 and Table 2 for the eccentricity = 0%. The discrepancy is defined as

$$\text{Discrepancy}(\%) = \frac{\text{frequency by FEM} - \text{theoretical frequency}}{\text{frequency by FEM}} \times 100 \quad (31)$$

The largest discrepancy between the theoretical and finite element analysis results is 2.7% for the mode of (1, 2). Discrepancies defined by Eq. (31) are always less than 3%, therefore the theoretical results agree well with finite element analysis results, verifying the validity of the analytical method developed.

Frequency comparisons for the eccentricity of 20% are shown in Fig. 5. Not like the case of the

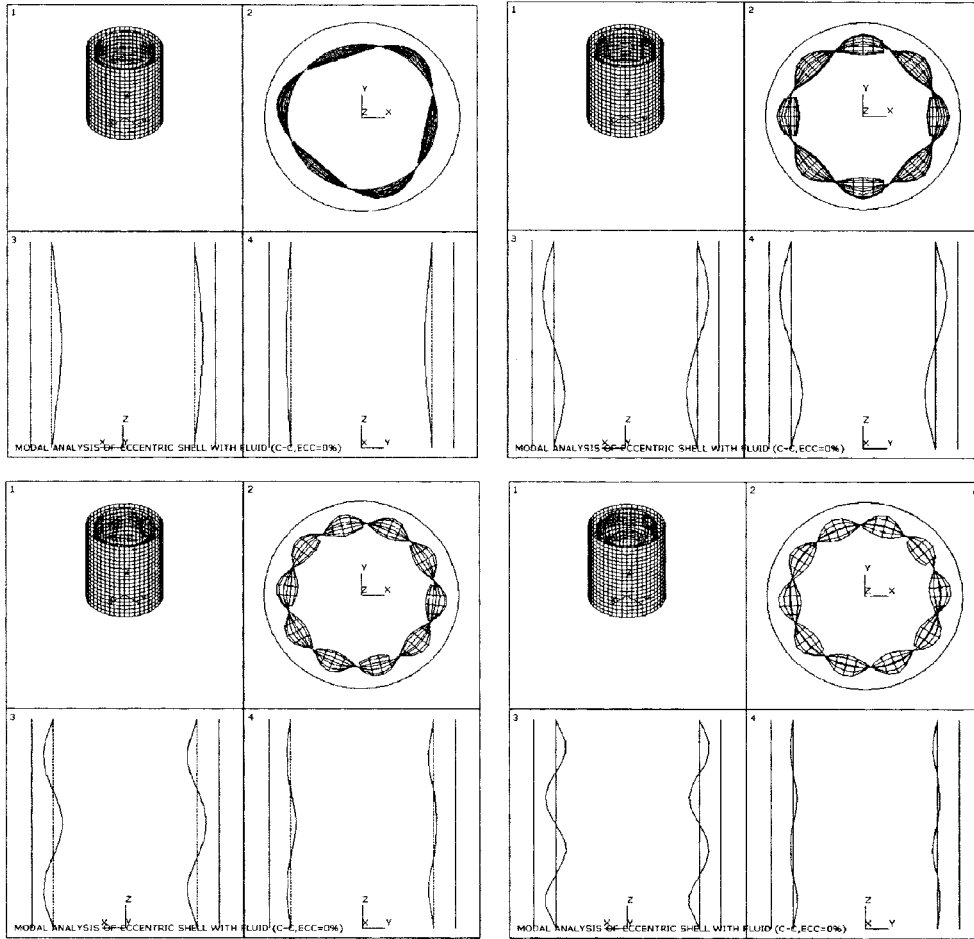


Fig. 3 Typical mode shapes for eccentricity = 0%

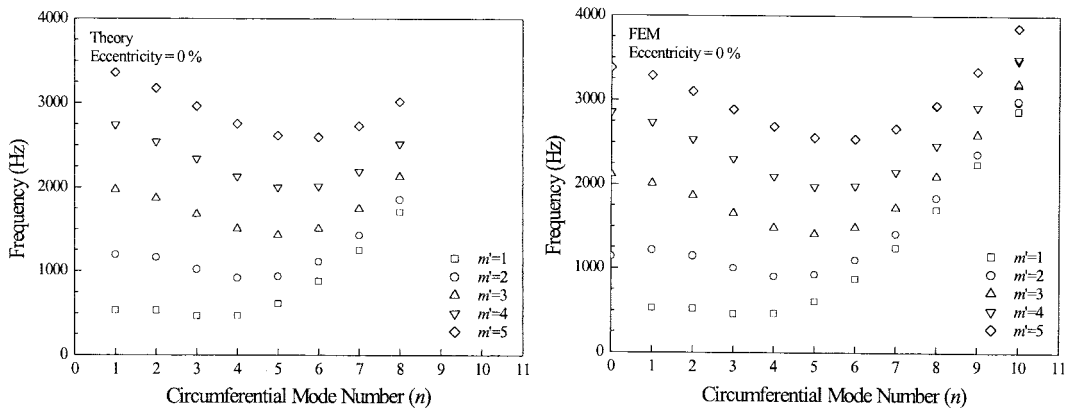


Fig. 4 Frequency comparisons for eccentricity = 0%

Table 2 Natural frequencies for eccentricity = 0%

Circumferential mode ( $n$ )	Axial mode ( $m'$ )	Frequency (Hz)		Discrepancy (%)
		Theory	FEM	
1	1	533	528	-0.95
	2	1195	1221	2.13
	3	1975	2015	1.99
	4	2744	2738	-0.22
	5	3362	3289	-2.22
2	1	535	521	-2.69
	2	1163	1150	-1.13
	3	1872	1868	-2.14
	4	2545	2539	-2.36
	5	3177	3101	-2.45
3	1	469	459	-2.18
	2	1021	1004	-1.69
	3	1680	1659	-1.27
	4	2344	2308	-1.56
	5	2962	2888	-2.56
4	1	471	465	-1.29
	2	919	908	-1.21
	3	1503	1484	-1.28
	4	2132	2098	-1.62
	5	2754	2689	-2.42
5	1	612	607	-0.82
	2	937	928	-0.10
	3	1429	1414	-1.06
	4	2005	1976	-1.47
	5	2614	2560	-2.11
6	1	880	876	-0.05
	2	1111	1102	-0.08
	3	1507	1491	-1.07
	4	2018	1988	-1.51
	5	2596	2544	-2.04
7	1	1249	1246	-0.02
	2	1427	1416	-0.08
	3	1747	1726	-1.22
	4	2192	2154	-1.76
	5	2729	2668	-2.29
8	1	1707	1704	-0.18
	2	1858	1844	-0.08
	3	2130	2100	-1.43
	4	2520	2471	-1.98
	5	3017	2938	-2.69

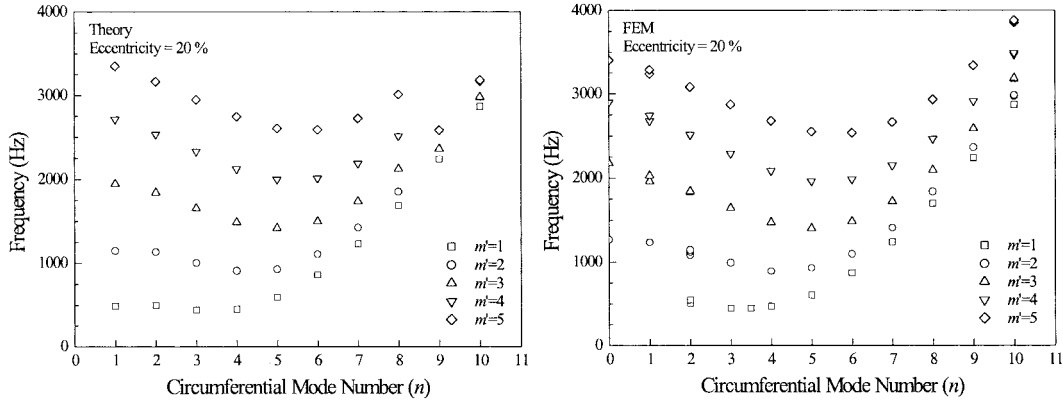


Fig. 5 Frequency comparisons for eccentricity = 20%

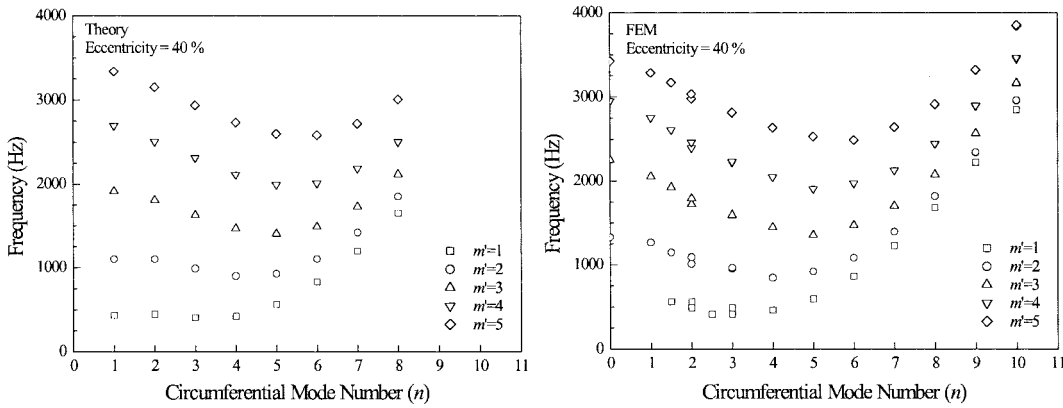


Fig. 6 Frequency comparisons for eccentricity = 40%

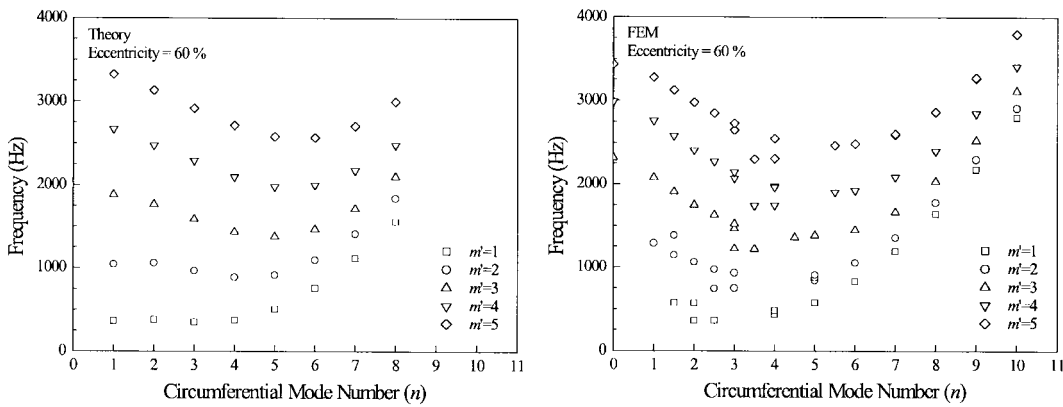


Fig. 7 Frequency comparisons for eccentricity = 60%

0% eccentricity, there are several points to be noted. No (1, 1) mode appeared in the finite element analysis and also modes of (2, 1), (1, 2) and (2, 2) have rather large discrepancies even though they

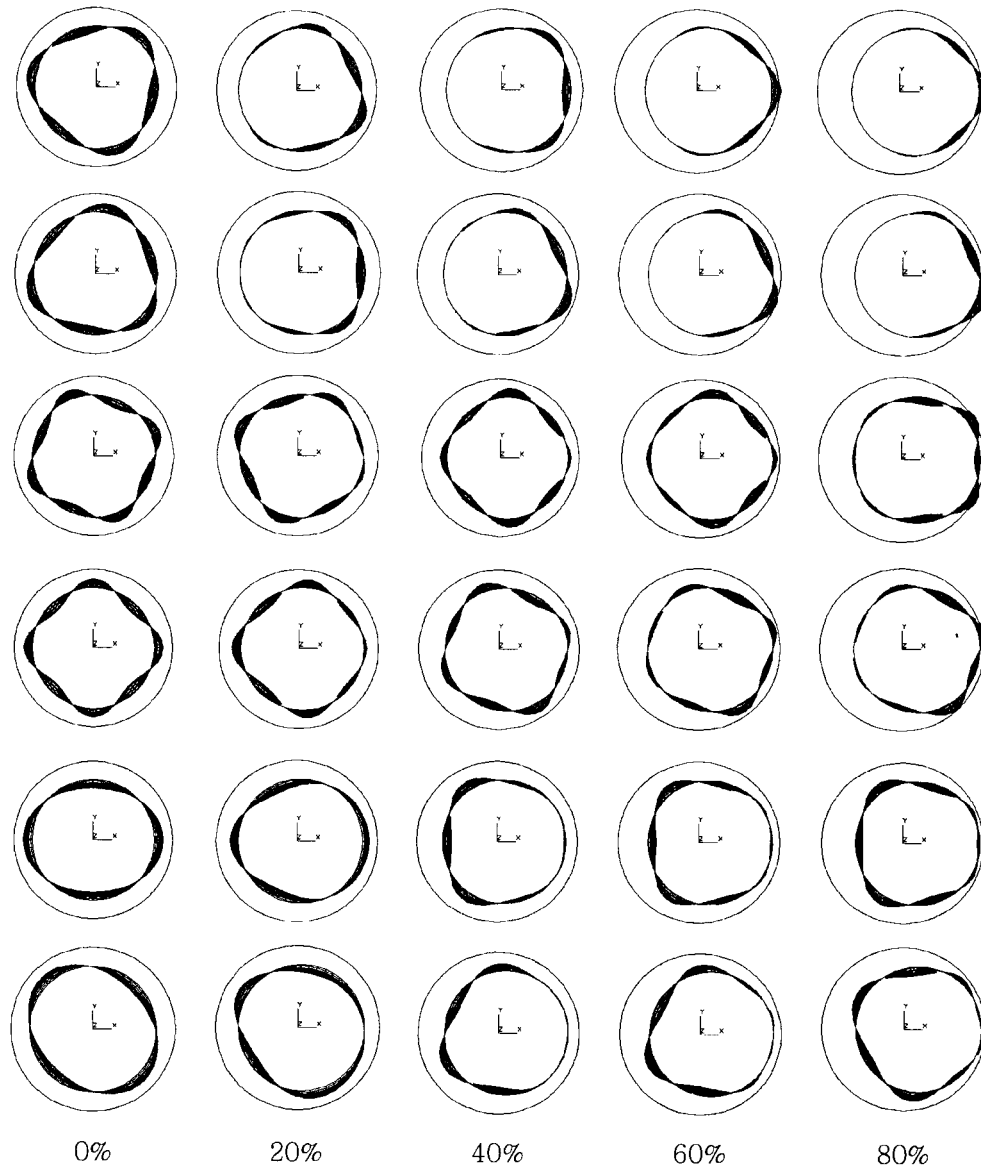


Fig. 8 Variation of mode shapes for  $m' = 1$  with respect to eccentricity

are within 10%. This is because (1, 1) mode for 0% eccentricity tends to move to adjacent modes such as (1, 2) or (2, 1) for the case of the 20% eccentricity. Also, (1, 3.5) mode of 445 Hz appeared, which is in progress of mode conversion from (1, 3) to (1, 4) modes. This kind of mode conversion, mode movement from lower to higher mode, is more evident as eccentricity becomes larger as shown in Figs. 6 and 7 for the eccentricities of 40% and 60%, respectively.

The variation of mode shapes with respect to eccentricity for axial mode  $m' = 1$  is shown for the first 12 modes in Fig. 8, which shows that some modes move to another modes with the change of eccentricity. For example one pair of (1, 4) mode appeared in the eccentricity of 40% or less, but

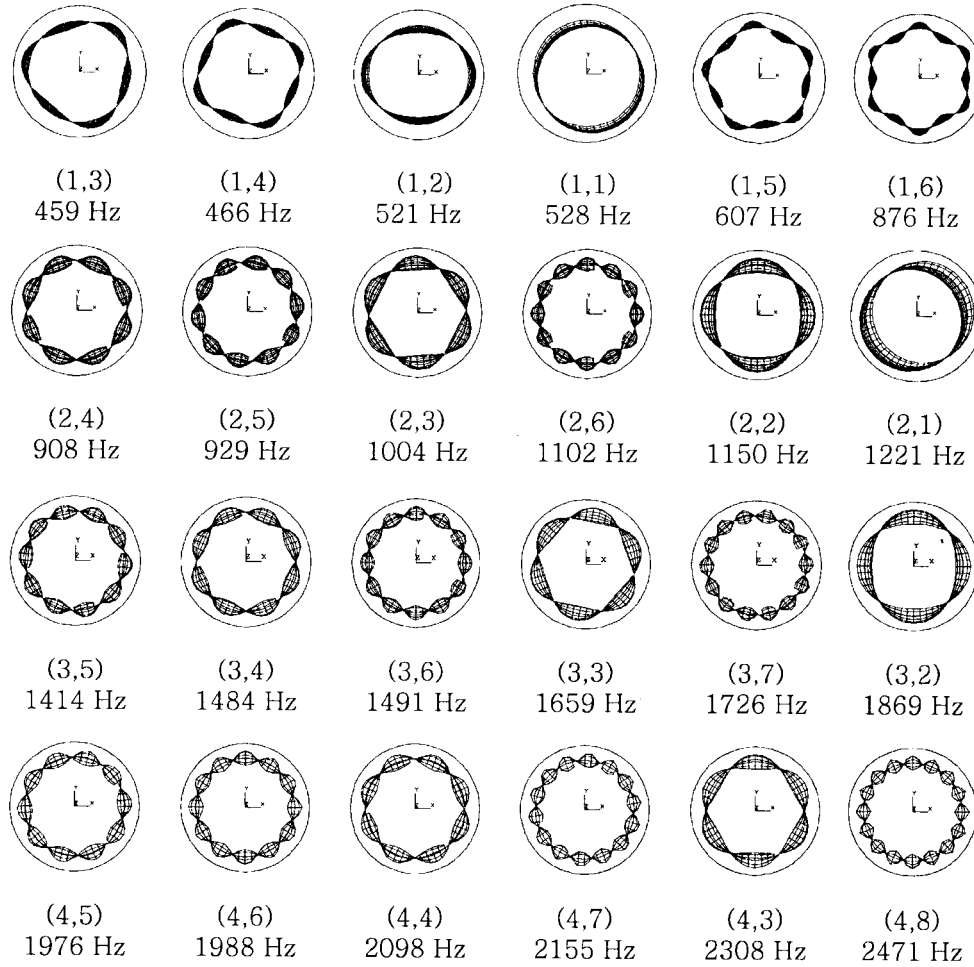


Fig. 9 Mode shapes for eccentricity = 0%

there are two pairs of (1, 4) modes in the eccentricity of 60%; one is the original (1, 4) mode of 40% eccentricity and the other is the conversion mode from (1, 3) of 40% eccentricity. Also, two pairs of (1, 2) modes appeared in the eccentricity of 20%; one is original (1, 2) mode and the other is the mode from (1, 1) mode of the 0% eccentricity. This kind of mode movement with larger eccentricity is the cause of the appearance of several circumferential mode number of order 0.5, and also the reason for not appearing of several modes such as (1, 1) mode for eccentricities of 20% and (2, 4) mode for eccentricities of 60%.

Because there is unsymmetric configuration for shells with eccentricity, there should be unsymmetric modes for certain modes. This trend is much more severe with large eccentricity except for circumferential and/or axial modes. Two separate values of mode are obtained especially for circumferential mode number  $n \leq 2$  in eccentricity = 20%,  $n \leq 3$  in eccentricity = 40% and  $n \leq 5$  in eccentricity = 60%. Contrary to this, modes for the eccentricity = 0% have exactly the same symmetric mode shapes for all modes as shown in Fig. 9.

Fig. 10 shows the variation of frequency values with respect to the eccentricity for several modes

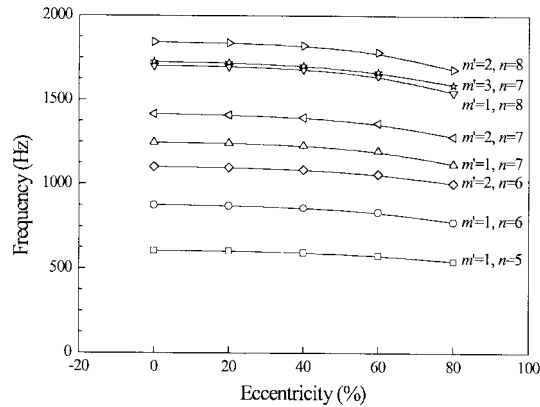


Fig. 10 Variation of frequencies with respect to eccentricity

which are not much affected by the eccentricity. If there is no mode conversion with increasing eccentricity, the effect of eccentricity on the frequencies is almost negligible, which is especially true for the high circumferential modes. Therefore the eccentricity is found to be more effective on the separation of modes or mode conversion than on the change of the frequencies.

## 5. Conclusions

An analytical method to estimate the coupled frequencies of the cylindrical shells with fluid-filled annulus is developed using the series expansion method based on the Fourier transformation. To verify the validity of the analytical method developed, finite element method is used and the frequency comparisons between them are found to be in good agreement, especially for the eccentricity of 0%. With the increasing eccentricity some modes are separated or mode conversions are found, which is not incorporated in the theoretical development. This needs to be studied in the future to define more sophisticated modes such as the circumferential mode of order 0.5. But in general the theory developed agrees well with the finite element method except for several transition modes which are changing with eccentricity. The effect of the eccentricity on the frequencies is found to be more severe on the appearance of transition modes or disappearance of certain modes rather than on the frequency changes. Therefore it is recommended to investigate the modal characteristics rather than frequency itself to know that how much eccentricity is there in the shells with fluid-filled annulus.

## References

- ANSYS (1998), *ANSYS Structural Analysis Guide*, ANSYS, Inc., Houston.  
 Chen, S.S. and Rosenberg, G.S. (1975), "Dynamics of a coupled shell-fluid system", *Nuclear Engineering and Design*, **32**, 302-310.  
 Chung, H. (1981), "Free vibration analysis of circular cylindrical shells", *J. Sound Vib.*, **74**, 331-350.  
 Danila, E.B., Conoir, J.M. and Izbicki, J.L. (1995), "The generalized Debye series expansion : treatment of the

- concentric and non-concentric cylindrical fluid-fluid interfaces”, *J. Acoust. Soc. Am.*, **98**, 3326-3342.
- Jeong, K.H. (1998), “Natural frequencies and mode shapes of two coaxial cylindrical shells coupled with bounded compressible fluid”, *J. Sound Vib.*, **215**, 105-124.
- Jeong, K.H. and Kim, K.J. (1998), “Free vibration of a circular cylindrical shell filled with bounded compressible fluid”, *J. Sound Vib.*, **217**, 197-221.
- Jeong, K.H. and Lee, S.C. (1996), “Fourier series expansion method for free vibration analysis of either a partially fluid-filled or a partially fluid-surrounded circular cylindrical shell”, *Comput. & Struct.*, **58**, 937-946.
- Jhung, M.J. (1996), “Shell response of core barrel for tributary pipe break”, *Int. J. Pressure Vessels and Piping*, **69**(2), 175-183.
- Jhung, M.J. (2000), *Modal analysis of coaxial shells with fluid-filled annulus*, KINS/RR-021, Korea Institute of Nuclear Safety.
- Sneddon, N. (1951), *Fourier Transforms*, McGraw-Hill Book, New York.
- Song, S.H. and Jhung, M.J. (1999), “Experimental modal analysis on the core support barrel of reactor internals using a scale model”, *KSME Int. J.*, **13**(8), 585-594.
- Watson, G.N. (1980), *A Treatise on the Theory of Bessel Functions*, second edition, Cambridge University Press, Cambridge.
- Yoshikawa, S., Williams, E.G. and Washburn, K.B. (1994), “Vibration of two concentric submerged cylindrical shells coupled by the entrained fluid”, *J. Acoust. Soc. Am.*, **95**, 3273-3286.